

Enhanced hexavalent chromium adsorption from aqueous solutions onto amine functionalized MWCNTs synthesized using iron(0)/egg-shell as an efficient catalyst

Hassan Alijani^a, Zahra Shariatinia^{a,*}, Abdolreza Aroujalian^b

^aDepartment of Chemistry, Amirkabir University of Technology (Tehran Polytechnic), P.O. Box 15875-4413, Tehran, Iran, Tel. +98 2164542766; Fax: +98 2164542762; emails: shariati@aut.ac.ir, shariatiz@yahoo.com (Z. Shariatinia), alijani.hassan89@gmail.com (H. Alijani)

^bDepartment of Chemical Engineering, Amirkabir University of Technology (Tehran Polytechnic), P.O. Box 15875-4413, Tehran, Iran, email: aroujali@aut.ac.ir (A. Aroujalian)

Received 14 April 2016; Accepted 23 June 2016

ABSTRACT

Multiwall carbon nanotubes (MWCNTs) were synthesized using chemical vapor deposition method by iron impregnation onto the natural egg-shell support. The employed support has a low cost and the iron fragment induces superparamagnetic property on as-synthesized MWCNTs which were then functionalized with ethylenediamine (En) as well as triethylenetetramine (TTA). The prepared materials were characterized by XRD, TGA/DTA, VSM, FT-IR and Raman techniques. Effect of iron percentage on the MWCNT yield and influence of temperature on the product quality were investigated. The as-synthesized MWCNTs, oxidized MWCNTs and amine functionalized MWCNTs were employed for Cr(VI) removal from aqueous solution. Effective parameters on adsorption efficiency such as pH, contact time, adsorbent dosage and temperature were optimized. Kinetic and isotherm studies revealed that chromium adsorption by modified adsorbents followed second order and Langmuir adsorption model with the equilibrium time of 30 min and adsorption capacities of 125 and 166.6 mg g⁻¹ using MWCNTs and oxidized CNTs, respectively, while 333.3 mg g⁻¹ using both amine functionalized MWCNTs. Thermodynamic experiments illustrated that chromium adsorption was spontaneous as well as followed an exothermic path. Regeneration of the sorbents using NaOH solution exhibited that the sorbents have appropriate reusabilities after six cycles of sorption and desorption.

Keywords: Carbon nanotube; Chemical vapor deposition; Chromium(VI) removal; Natural egg-shell support

1. Introduction

Water contamination by heavy metals is believed to be one of the most significant environmental problems due to the excessive release of industrial effluents as a result of rapid industrial development. Heavy metals are highly hazardous to environment and ecosystem even at low con-

centration levels [1,2]. Among heavy metals, hexavalent chromium has been considered to be a highly toxic and potentially carcinogenic ion which has caused serious health problems [3]. Cr(VI) is rarely naturally occurring, relatively soluble in aqueous systems and is readily transformed in groundwater [4]. The US Environmental Protection Agency (EPA) and the World Health Organization (WHO) recommended a maximum concentration of 100 µg/L and 50 µg/L for the total chromium and Cr(VI) in drinking water, respectively [5]. Consequently, it is required to

*Corresponding author.

reduce Cr(VI) concentration to an acceptable level in order to avoid the threats to public health [6].

Hitherto, various removal methods have been developed for removing Cr(VI) including chemical precipitation, membrane separation, ion exchange and adsorption. Most of these methods are effective but require a large quantity of chemicals and/or high energy; however, adsorption considered to be as one of the most promising technology due to its high efficiency, low technological equipment, reusability of the adsorbents and flexibility of design [7–9]. It is known that selection of adsorbent is a key factor which affects the efficiency of the adsorption technique. Recently, it has been revealed that nanotechnology can resolve many issues involving environmental pollution by highly efficient and cost-effective approaches [10]. Accordingly, several nanoadsorbents such as nanoclay [11,12], polymer nanocomposite [13–16], ionic liquid [17], activated carbon [18] and magnetic nanocomposite [19] have been tested with the aim of removing the chromium pollutants from wastewater. In spite of the fact that these materials have been useful for the end of remediation, most of them are not so efficient. Among nanostructure compounds, carbonaceous nanomaterials especially graphene and carbon nanotubes attracted more attention as very popular advanced materials. Multiwalled carbon nanotubes (MWNTs) were recognized as the efficient adsorbents for the removal of organic and inorganic contaminants, either in their oxidized form or in conjunction with other materials [20]. Their small sizes, large surface areas, high mechanical strength and surface modification possibility have caused their fabulous potentials for waste treatment [21]. On the other hand, collection times associated with carbonaceous compounds from aqueous solution are excessive, resulting in loss of adsorbents. Therefore, there is still a requirement for the development of an efficient adsorbent having high adsorption efficiency for Cr(VI) removal. Preferably, it would be more advantageous if the MWCNT could magnetically be recovered from solution. Also, surface functionalization of MWCNT is another approach to improve its properties. Carbon materials are usually functionalized by oxidative processes to change the sidewalls and tube tips so that carboxylation by acidic groups is a common reaction process [22,23]. In the subsequent step, it can further be modified with desired functional groups to improve its surface reactivity.

Based on the above facts, we have prepared magnetic MWCNTs (on egg-shell as a substrate) and amine functionalized MWCNTs for adsorption of chromium(VI) from aqueous solution. MWCNTs have been synthesized by chemical vapor deposition (CVD) method as an efficient and scalable synthetic route. Moreover, iron(0)/egg-shell catalyst, composed of CaCO_3 , was used as a substrate material to synthesize an efficient catalyst for the MWCNTs synthesis. The role of egg-shell is to disperse the catalyst active phase and prevent its aggregating into large clusters. Egg-shell has a low cost and is readily available as a mineral as well as easily removed from final product by acid treatment; therefore, it is a good candidate to be employed as a substrate for the CNTs synthesis. The as-synthesized MWCNTs, oxidized MWCNTs, and two types of amine functionalized MWCNTs prepared using ethylenediamine (En) and triethylenetetramine (TTA) were employed for effective removal of aqueous Cr(VI). Important parameters on chromium

adsorption were optimized, and kinetic, isotherm and thermodynamic behaviors were also investigated.

2. Experimental section

2.1. Materials and instruments

Egg-shell was powdered and washed with distilled water, then dried at 50°C for 5 h and sieved. $\text{Fe}(\text{NO}_3)_3 \cdot 9\text{H}_2\text{O}$ (Merck, Darmstadt, Germany) was used as the iron source. Standard solutions of chromium(VI) ions (1,000 mg L⁻¹) were prepared by dissolving $\text{K}_2\text{Cr}_2\text{O}_7$ salt in a minimum amount of HNO_3 and then diluting to appropriate volumes with distilled water. The pH adjustment was performed using 0.1 mol L⁻¹ HNO_3 and 0.1 mol L⁻¹ NH_3 solutions.

Prepared materials were characterized by X-ray diffraction (XRD) patterns which were recorded on a Philips-X'pertpro X-ray diffractometer. Scanning electron microscopy (SEM) images were obtained using LEO-1455VP instrument. Micro-Raman spectra were recorded on a Renishaw system 1000 spectrometer, equipped with Leica DMLM microscope, a 25-mW diode laser (782 nm), and a CCD detector. Transmission electron microscopy (TEM) was carried out on a LEO 912AB instrument under an accelerated voltage of 120 kV. Fourier transform infrared spectra (FT-IR) were measured with Equinox 55 Bruker instrument with ATR method over the wavelength of 400–4,000 cm⁻¹. Thermal gravimetric analysis/differential thermal analysis (TGA/DTA) and vibrational sample magnetometer (VSM) diagrams were recorded with a TA-Q-50 and Lake Shore Model 7400 (Japan) instruments, respectively.

2.2. Synthesis of catalyst and MWCNTs

To prepare the natural egg-shell supported iron(0) catalyst, an appropriate amount of $\text{Fe}(\text{NO}_3)_3 \cdot 9\text{H}_2\text{O}$ was dissolved in 200 mL methanol and 5.0 g of substrate (egg-shell powder) was added to this solution. The final mixture was stirred for 2 h and filtered with filter paper, then dried at 200°C for 2 h. The final product was calcined at 500°C for 4 h. The catalyst metal loading amounts were 5%, 10%, and 15% w/w of iron with respect to the egg-shell.

Synthesis of MWCNTs was performed in the presence of egg-shell supported iron catalyst. For this purpose, about 0.2 g of the catalyst powder was placed in the quartz reactor with an internal diameter of 46 mm and external diameter of 50 mm, and a length of about 880 mm equipped with a thermocouple located in the catalyst bed. The reactor was moved to a furnace and purged with argon till the reactor was reaching 700°C–800°C as the synthesis temperatures. After that, the argon flow was stopped and methane stream was opened and continued for 30 min with a rate of 50 mL min⁻¹. At the end of the reaction, the methane stream was switched back to argon until the temperature reached to ambient temperature and the samples were collected for further analysis.

2.3. Functionalization of MWCNTs

In order to activate the MWCNTs surfaces, about 1.0 g of MWCNT material (synthesized at 800°C using 15% catalyst) was added to 20 mL concentrated nitric acid and sonicated

for 1 h, then the mixture was stirred overnight at room temperature. After that, it was filtrated and rinsed with distilled water until the pH of the suspension reached about the neutral value and then the powder was dried at 80°C for 5 h. In the subsequent step to acylation of CNTs, the oxidized CNTs (0.4 g) was added to a mixture of thionyl chloride (5 mL) and DMF (50 mL) and was stirred for 6 h at 40°C. The resulting mixture was filtered, washed with DMF and magnetically dispersed in 50 mL DMF followed by dropping of 5 mL En and TTA to it. After refluxing for 6 h at 60°C, modified CNTs was separated by filtration, washed with ethanol and distilled water and dried in an oven at 70°C for 5 h.

2.4. Adsorption experiments

The chromium(VI) adsorption was carried out using CNTs, oxidized CNTs (CNTs-COOH), CNTs-En, and CNTs-TTA adsorbents. Adequate amounts of the adsorbents (0.15 g L⁻¹) were added to a series of 50 mL

sample solutions of chromium(VI) with the concentration of 20 mg L⁻¹. The pH of sample mixtures was adjusted to 2.5 by using diluted solutions of HCl and NH₃. After shaking for 30 min, the adsorbents were separated magnetically and residual chromium(VI) concentrations in the supernatants were determined by ICP-AES analysis.

3. Results and discussion

3.1. Characterization of materials

The XRD characterization was employed to identify the structures of the egg-shell, catalyst with a metal loading of 15 wt.% and as-synthesized CNTs at 800°C. According to the results (Fig. 1(a)), the XRD pattern of egg-shell has the diffraction peaks which are much similar to those of the calcite phase. The high intense peak at $2\theta = 29^\circ$ is along with the 104 plane of calcite; however, low reflections of aragonite at $2\theta = 27, 32,$ and 43° are also observable [24,25].

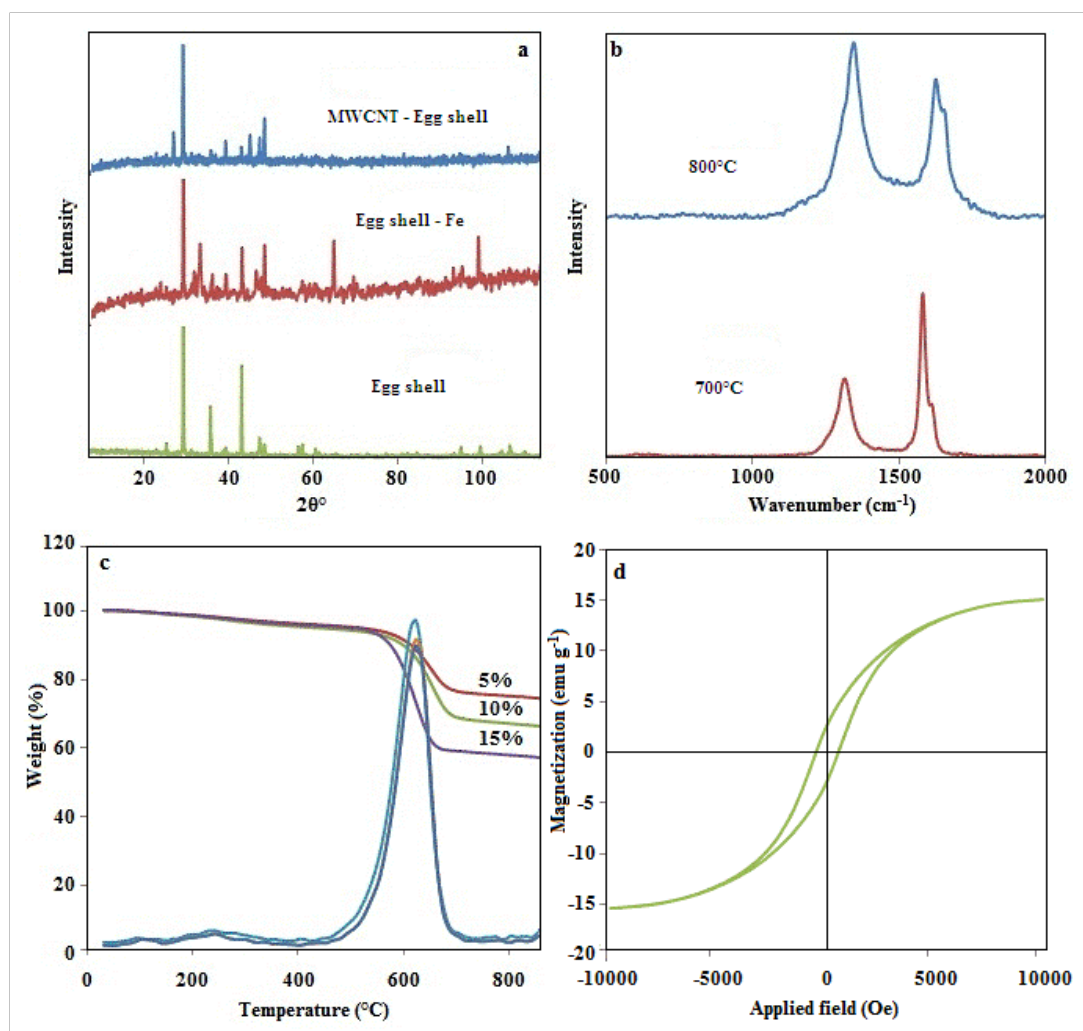


Fig. 1. The XRD patterns of egg-shell: (a) iron-doped egg-shell and MWCNTs synthesized using 15% catalyst at 800°C, (b) Raman spectra of MWCNTs synthesized using 15% catalyst at 700°C and 800°C, (c) TGA/DTA diagrams of MWCNTs synthesized using 5%, 10%, 15% catalysts at 800°C, and (d) VSM graph of MWCNTs synthesized using 15% catalyst at 800°C.

The XRD pattern of catalyst shows some differences with regard to egg-shell pattern which is owing to the formation of Fe_2O_3 phase in the substrate matrix. As can be seen, the pattern demonstrates new scatterings at 2θ values of 24° , 34.1° , 50.52° and 63.2° due to the crystal structure that can be indexed to the (012), (104), (024), and (214) rhombohedral lattice of hematite [26]. Moreover, it can be seen that the intensities of aragonite peaks are decreased; however, calcite do not illustrate change in peak intensity which may be owing to the more stability of calcite than aragonite. After synthesis of CNTs on the catalyst surface, a main change is observed in the XRD pattern with appearing the peak at the 2θ equal to 27.2° . This peak is related to the growth of MWCNTs on the surface of catalyst and originated from the graphite lamellar structure of CNTs. Another change in the XRD pattern corresponds to the disappearing of peaks associated with hematite phase as only the peak at 2θ equal to 45° has been unchanged. This peak is matched to (110) plane of zero valent iron nanoparticles [27,28]. In other words, the peak is owing to phase change of hematite within synthetic process which generates zero valent iron nanoparticles that in the subsequent step, they catalyze the growth of MWCNT on the surface of substrate. Zerovalent iron nanoparticles are generated by reduction of hematite with released hydrogen (H_2) as a result of thermal cracking of methane.

Raman spectroscopy is an efficient technique that is considered to be a very helpful method for CNTs characterization; moreover, this method is not time consuming, non-destructive as well as it is required a minimum amount of sample. The Raman spectra of MWCNTs synthesized using 15% catalyst at 700°C and 800°C are presented in Fig. 1(b). The spectra consist of D mode ($1,347\text{ cm}^{-1}$) or in-plane breathing mode of A_{1g} symmetry which is assigned to out-of-plane phonon modes in the low frequency region. Another peak includes G mode ($1,583\text{ cm}^{-1}$) or in-plane bond stretching motion of sp^2 hybridized carbon atoms [29]. According to the results, the Raman spectrum of MWCNTs synthesized at 700°C consists of one basic intensive G-band, corresponding to graphene structure of CNT, and another weaker D band due to amorphous or other disordered carbon structure. Furthermore, the intensity of D band is because of the high density of the aligned tubes as well as turbostratic structure of carbon sheets in nanotubes [30]. Another result which is extractable from the spectra is based on the I_G/I_D ratio. It is known that this ratio is proportional to the quality of nanotubes [31]. As can be seen, the intensity ratio of the G to D bands is decreased with increasing the reaction temperature. In other words, the qualities of CNTs are decreased as well as the degree of disorder is increased at higher temperature. The main reason for this situation is owing to the deactivation of the catalyst by formation of amorphous carbonaceous species. In other words, at higher temperature (800°C), the dimensions of catalyst particles can be changed by sintering, thus large catalyst particles form which are less active to catalyze the growth of the CNTs; hence, they induce formation of amorphous carbon. Disorders in CNTs structures offer an appropriate situation for increasing acidic centers on their surfaces with acid treatment which finally improve metal adsorption properties of as-synthesized CNTs. Therefore, synthesized CNTs at 800°C were used for surface modification and chromium(VI) adsorption experiments.

The TGA technique was used to investigate the effect of catalyst amount on CNTs yield as well as the purity of the synthesized CNTs. Fig. 1(c) shows TGA/DTA diagrams of as-synthesized CNT by adding 5%, 10% and 15% of iron to the egg-shell substrate at 800°C and reaction time of 30 min. According to the data, one major weight loss appears in the range of 500°C – 700°C with a central point near 600°C . In addition, it can be seen that no significant weight loss is appeared at temperatures lower than 400°C which confirms that low amounts of amorphous carbon is present in the product, since combustion of amorphous carbon usually occurs below 450°C , while the CNTs burn at a higher temperature [32]. The increase in CNTs yield with increasing the catalyst amount is owing to the feasibility of methane cracking at higher level of catalyst amount. In other words, hydrogen generation by methane cracking induces production of more zerovalent iron nanoparticles as active catalyst fragments for the CNTs synthesis. Based on the above descriptions, CNTs synthesized in the presence of 15% iron were selected for chromium(VI) adsorption experiments because more generation of iron nanoparticles induces stronger magnetic characteristic on the product which facilitates its application as a magnetic adsorbent.

The magnetic hysteresis loops of the MWCNTs synthesized using 15% catalyst at 800°C is displayed in Fig. 1(d). The saturated magnetization of the composite was 15.6 emu g^{-1} as well as the remanence value was 0.068 emu g^{-1} , indicating that the material has a superparamagnetic property. Magnetic behavior of the sorbent is originated from the iron phase in the CNTs channels. In fact, hematite particles are converted to iron nanoparticles which induce magnetic property onto the composite. Based on the result, as-synthesized material has a good magnetic property to be employed as a magnetic adsorbent.

The FT-IR spectra of oxidized CNT and amine functionalized adsorbents are demonstrated in Fig. 2.

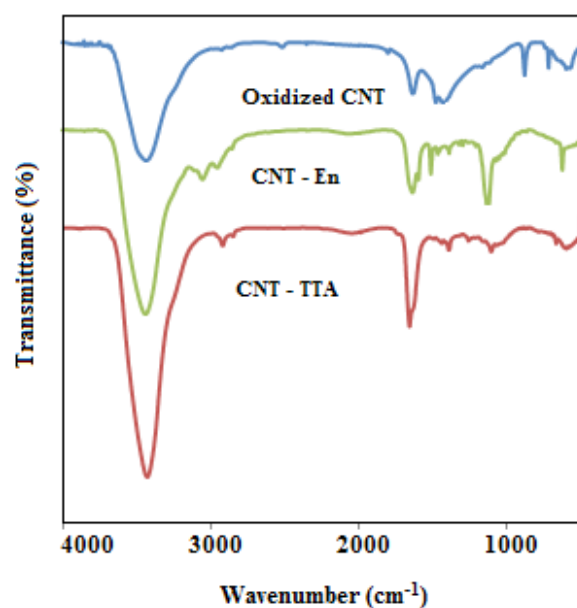


Fig. 2. The FT-IR spectra of oxidized CNT (synthesized using 15% catalyst at 800°C) and amine functionalized materials.

Several characteristic bands are observable in the spectra of oxidized CNTs. The bands at 1,082 and 855 cm^{-1} are assigned to substituted aromatic ring and C–H out-of-plane bending vibrations, respectively [33]. Other characteristic bands include –CH and –OH vibrations at 2,900 and 3,000–3,500 cm^{-1} . The peaks corresponding to C=C stretching in the CNTs structure are appeared within the range of 1,100–1,500 cm^{-1} . Furthermore, the band at 1,630 cm^{-1} are assigned to –C=O stretching vibrations [34]. After amine functionalization, the intensities of –CH (at around 2,940 cm^{-1}) and –NH amine (near 3,400 cm^{-1}) vibrations are increased owing to the presence of En and tetramine on the surfaces of as-modified CNTs.

The morphology and structure of egg-shell as well as synthesized CNTs were studied by SEM analysis. Fig. 3(a) reveals the SEM images of the egg-shell substrate. It can be seen that the material is in macro level with a high porosity in its surface. This structure can provide a high surface for adsorbing Fe^{3+} ions as in the subsequent step, the zerovalent iron can easily be dispersed on the substrate matrix and prevent agglomeration of the catalyst particles. The SEM micrograph of CNTs is given at Fig. 3(b). As can be seen, the CNTs appeared as some bundled structures composed of fine filaments. Bundles formation is a result of strong van der Waals interactions between individual nanotubes, which induce high tendency of CNTs to form bundled structures [35]. The TEM analysis (Figs. 3(c) and 3(d)) was also obtained for the MWCNTs synthesized using 15% catalyst at 800°C. It is observed that the catalyst particles exist as dark spots on/within the CNTs. Moreover, the images show that the prepared CNTs are appeared as segmentary structures with high purity and diameters in the range of 80–100 nm.

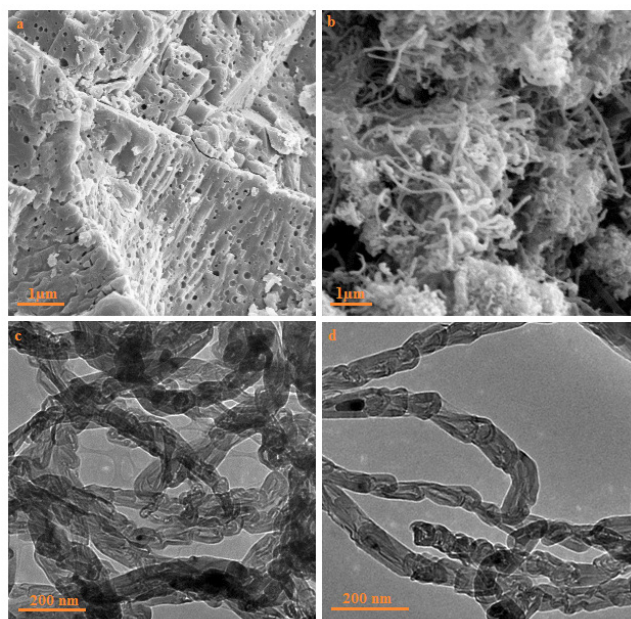


Fig. 3. The SEM micrographs of (a) egg-shell, (b) MWCNTs, and (c and d) TEM images of MWCNTs synthesized using 15% catalyst at 800°C.

3.2. Effect of pH

The pH of the solution is a main factor which affects both metal species and surface properties of sorbents; hence the efficiency of adsorption process is primarily affected by this parameter. In order to evaluate the influence of pH on chromium(VI) adsorption, the experiments were carried out in the pH range of 2.0–9.0 by keeping other variables constant. A series of 50 mL sample solutions (30 mgL^{-1}) with adsorbent amount of 0.2 g L^{-1} at several pH values were shaken for 90 min. Afterward, the sorbent was separated and removal percentage was calculated using following equation, where C_0 and C_e are the initial and equilibrium concentrations (mg L^{-1}) of target analyte in the solution.

$$R\% = (C_0 - C_e) \times 100 / C_0 \quad (1)$$

The results in Fig. 4(a) exhibits that the removal percentage is decreased with increase in working pH as maximum removals of chromium(VI) using four types of adsorbents are obtained at acidic solutions, that is, the pH = 2–3. The dependence of chromium(VI) sorption on pH is related to the Cr(VI) speciation and surface charge of the adsorbents. In fact, by changing pH of the solution, chromium is predicted to exist predominantly as various anionic species. Important Cr(VI) equilibrium reactions by pH change can be summarized as following equations [36–38].



At pH values higher than 3.0, the removal percentages are lower, which can be owing to the negative surface charge of the sorbents. In other words, the sorbents which contain amine and carboxylic acid groups followed ion-exchange mechanism as protons can be replaced with chromium(VI) species from the solution. According to equilibrium equations, at the studied pH range, HCrO_4^- and $\text{Cr}_2\text{O}_7^{2-}$ occur together but the HCrO_4^- is dominant as it composes 95% of chromium species at pH higher than 2. In brief, ion exchange which is one of the most important adsorption mechanisms can be depressed at pH higher than 3.0 as a result of high concentration of chromate anion and negative charge of sorbent surface which repulse each other.

3.3. Effect of adsorbent dosage

Optimization of the adsorbent dosage is a significant factor since this parameter can maximize the interactions between metal ions and adsorption sites of adsorbent. The effect of this parameter on the removal efficiency is illustrated in Fig. 4(b). It is observed that the removal efficiencies enhance greatly as the dosage of sorbents increases from 0.025 to 0.15 g L^{-1} , and then reach a steady state up to dosage of 0.2 g L^{-1} . Moreover, the removal percentage of chromium(VI) using all sorbents have revealed significant changes over the mentioned dosage rang. This situation can

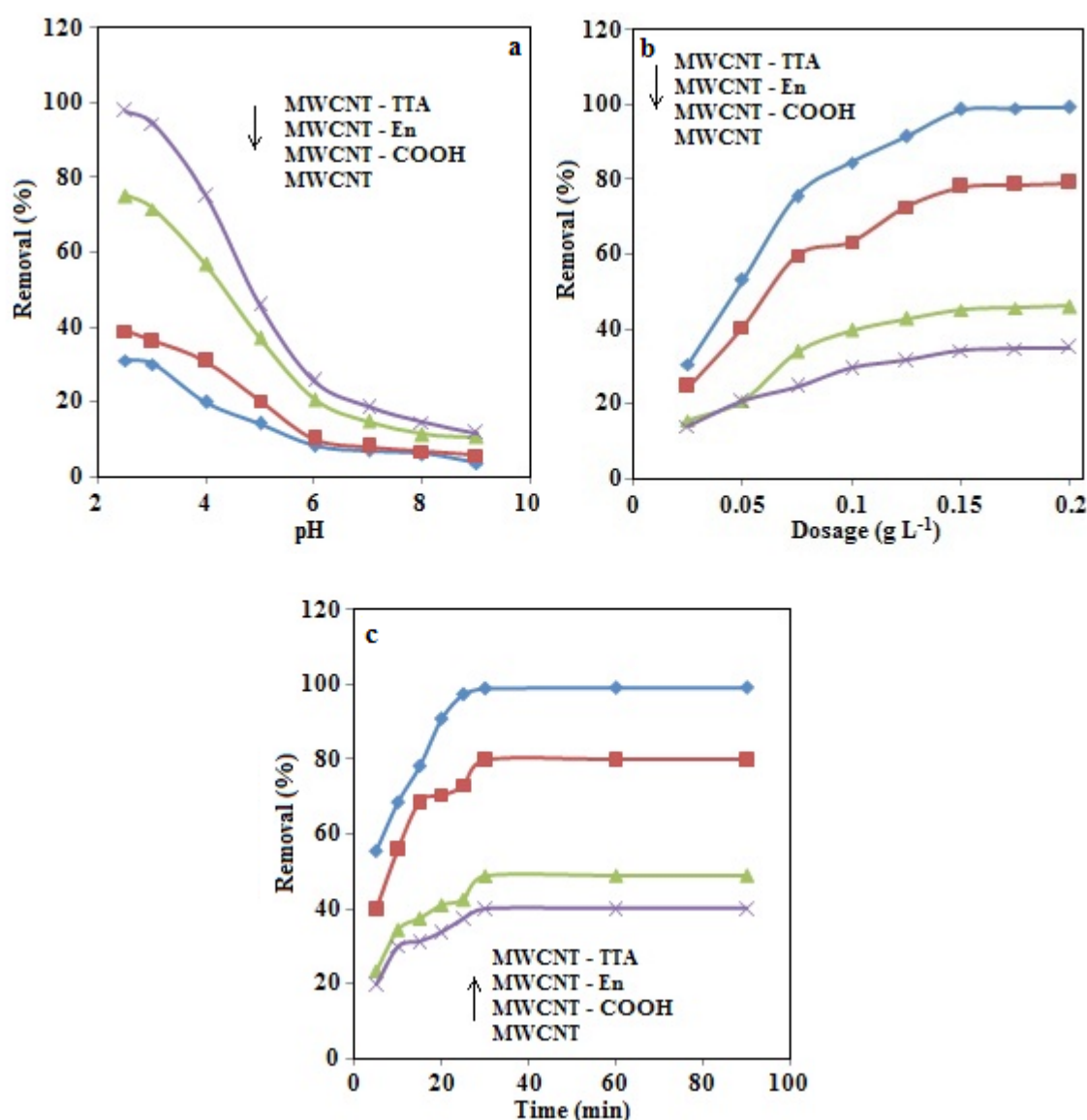


Fig. 4. Effect of pH (a) adsorbent dosage and (b) shaking time (c) on chromium adsorption.

be justified with the fact that the increase in the adsorbent dosage increases the surface active groups density; as a result, they can capture more amounts of metal ions. Steady state of removal percentage at higher adsorbent dosage can be owing to the aggregation of the adsorbent which causes removal efficiency reach a plateau. In other words, increasing adsorbent dosage impose a screening effect of the dense outer layer of the particles, thereby shielding the binding sites from analyte [39]. In order to obtain high removal efficiency, 0.15 g L⁻¹ was selected as the optimum adsorbent dosage for the experiments.

3.4. Effect of contact time and kinetic study

Chromium(VI) adsorption experiments with a Cr(VI) concentration of 10 mg L⁻¹ were performed within 5–90 min using CNT, CNT-COOH, CNT-En and CNT-TTA adsorbents. According to the results in Fig. 4(c), all sorbents show

the same uptake pattern but at the same experimental conditions, amine functionalized CNTs exhibit the highest efficiencies which reveal surface functionalization has positively modified adsorption properties of as-synthesized CNTs. Moreover, it can be seen that removal percentage is rapidly increased within the first 20 min and then, it is slowed down as the sites are gradually filled up. The first fast efficiency is due to the availability of a large number of adsorption sites. After this step, the kinetics will be more dependent on the rate at which the chromium(VI) ion is transported from the liquid phase to the adsorption sites. The increase in removal efficiency is not significant after 30 min, hence this time is selected for further work and confirms that chromium(VI) adsorption process follows fast equilibrium time. Such a fast adsorption rate could be attributed to the external surface adsorption, and absence of internal diffusion resistance.

Chromium(VI) adsorption properties of the sorbents were further investigated with two main kinetic models, that

is, the pseudo-first-order and pseudo-second-order models to quantify the changes in chromium(VI) adsorption with time. These models can be described with following linear equations, where K_1 and K_2 are the pseudo-first-order rate constant (min^{-1}) and pseudo-second-order rate constant of sorption ($\text{g mg}^{-1} \text{min}^{-1}$). Moreover, Q_e and Q_t represent the amount of analyte adsorbed at time t and at equilibrium (mg g^{-1}), respectively [40,41].

$$\ln(Q_e - Q_t) = \ln Q_e - K_1 t \quad (5)$$

$$t/Q_t = t/Q_e + 1/K_2 Q_e^2 \quad (6)$$

The parameters and plots based on the models at concentration level of 10 mg L^{-1} are listed in Table 1 and Fig. 5, respectively. It is observed that second-order model reveals high linearity with the same R^2 values using all types of adsorbents. The very high R^2 values (0.99) for pseudo-second-order expression suggests that this model may be appropriate to use for describing chromium(VI) adsorption properties of the sorbents. However, the results confirm that the Q_e obtained based on the first-order model, using raw CNTs as the adsorbent, has a lower deviation from experimental result compared with that achieved in the second-order model verifying the first-order model better describes chromium(VI) adsorption by raw CNTs.

On the other hand, the second-order model, using oxidized and functionalized sorbents, shows a lower deviation from experimental values relative to the first-order model; consequently, second-order model can be accepted as the kinetic mechanism for chromium(VI) adsorption using oxidized and functionalized adsorbents.

3.5. Isotherm study and error analysis

Results of the effect of initial chromium(VI) concentration in the range $0.5\text{--}80 \text{ mg L}^{-1}$ on removal percentage are presented in Fig. 6. It can be seen that the sorption by CNT-TTA is approximately complete (98.6%) at initial concentration of 20 mg L^{-1} . The efficiencies are 78%, 45% and 34% using CNT-En, CNT-COOH and CNT, respectively. These results confirm that at the same working situations, TTA functionalized CNT has the highest efficiency for chromium(VI) removal. At higher initial chromium(VI) concentration, the efficiency is decreased so that at initial concentration of 80 mg L^{-1} the removal percentage is 64%, 38%, 22% and 17% using CNT-TTA, CNT-En, CNT-COOH and CNT, respectively.

The effect of chromium(VI) concentration on the sorption was also analyzed in terms of Langmuir and Freundlich models. These models are expressed by the following linearized equations, where Q_e is the amount of metal ions adsorbed

Table 1
Data of first-order and second-order kinetic model for adsorption of chromium onto the adsorbents

Adsorbent	First order					Second order				
	R^2	Q	K_1	Q_{exp}	Deviation (%)	R^2	Q	K_2	Q_{exp}	Deviation (%)
CNT	0.96	23.78	0.091	26.82	-11.32	0.98	33.33	0.0038	26.82	+ 24.28
CNT-COOH	0.97	21.58	0.068	32.71	-34.02	0.99	35.71	0.0051	32.71	+ 9.17
CNT-En	0.95	37.18	0.088	53.46	-30.45	0.99	58.82	0.004	53.46	+ 10.02
CNT-TTA	0.89	93.87	0.16	66.15	+41.90	0.99	71.42	0.0037	66.15	+ 7.96

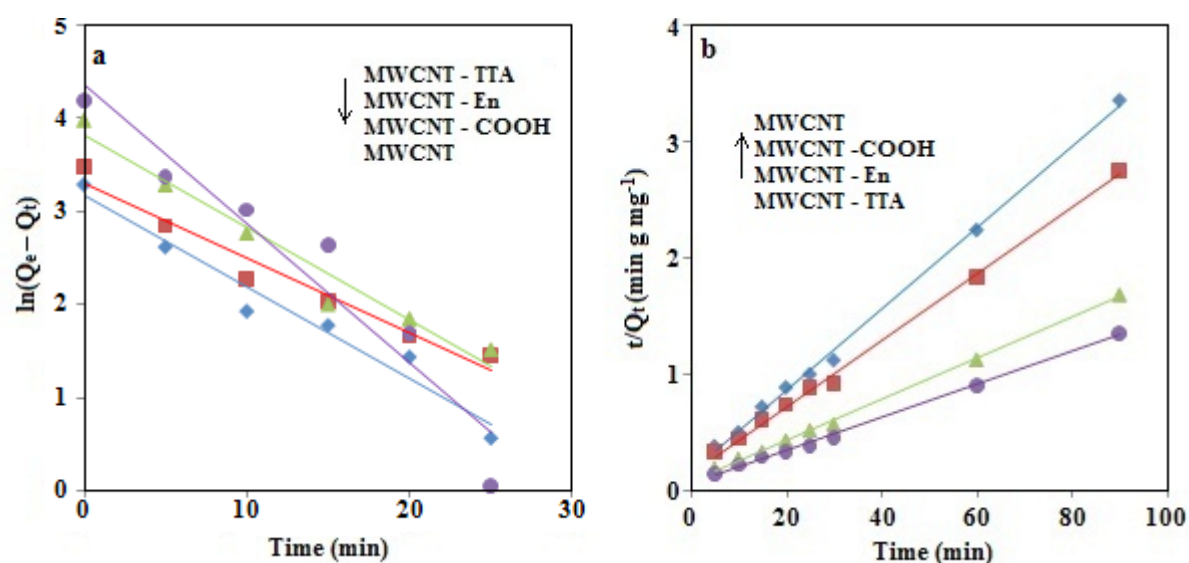


Fig. 5. (a) First-order and (b) second-order kinetic plots for chromium adsorption by as-synthesized materials.

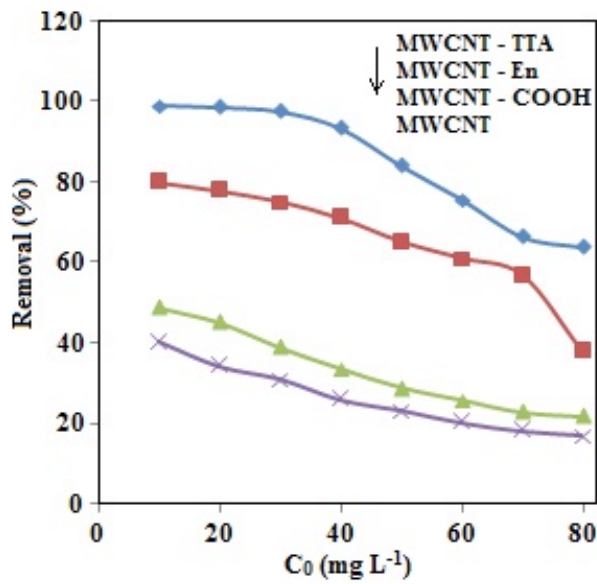


Fig. 6. Effect of initial chromium adsorption on the adsorption efficiency of adsorbents.

per unit mass of the sorbent (mg g^{-1}) and C_e is the amount of metal ions in the liquid phase at equilibrium (mg L^{-1}). The Q_m is the maximum adsorption capacity, b is Langmuir constant and K_f and n , are Freundlich coefficients [42–45].

$$1 / Q_e = 1 / (C_e Q_m b) + 1 / Q_m \tag{7}$$

$$\log Q_e = \log K_f + 1/n \log C_e \tag{8}$$

The curves of Langmuir and Freundlich models are depicted in Figs. 7(a)–(d) and the data are depicted in Table 2. According to the results, Langmuir model reveals the best fit relative to the Freundlich model because it exhibits relatively higher R^2 values. However, Freundlich model also shows approximately good linearities, but the linearities are lower than those of the Langmuir model, hence it may be concluded that the adsorption process does not follow Freundlich model. The accuracy of the suggestion is further evaluated by chi-square test (χ^2). This error function is given as Eq. (9), where Q_{exp} and Q_c are the experimental and calculated data from nonlinear models [46].

$$\chi^2 = \sum \frac{(Q_{\text{exp}} - Q_c)^2}{Q_c} \tag{9}$$

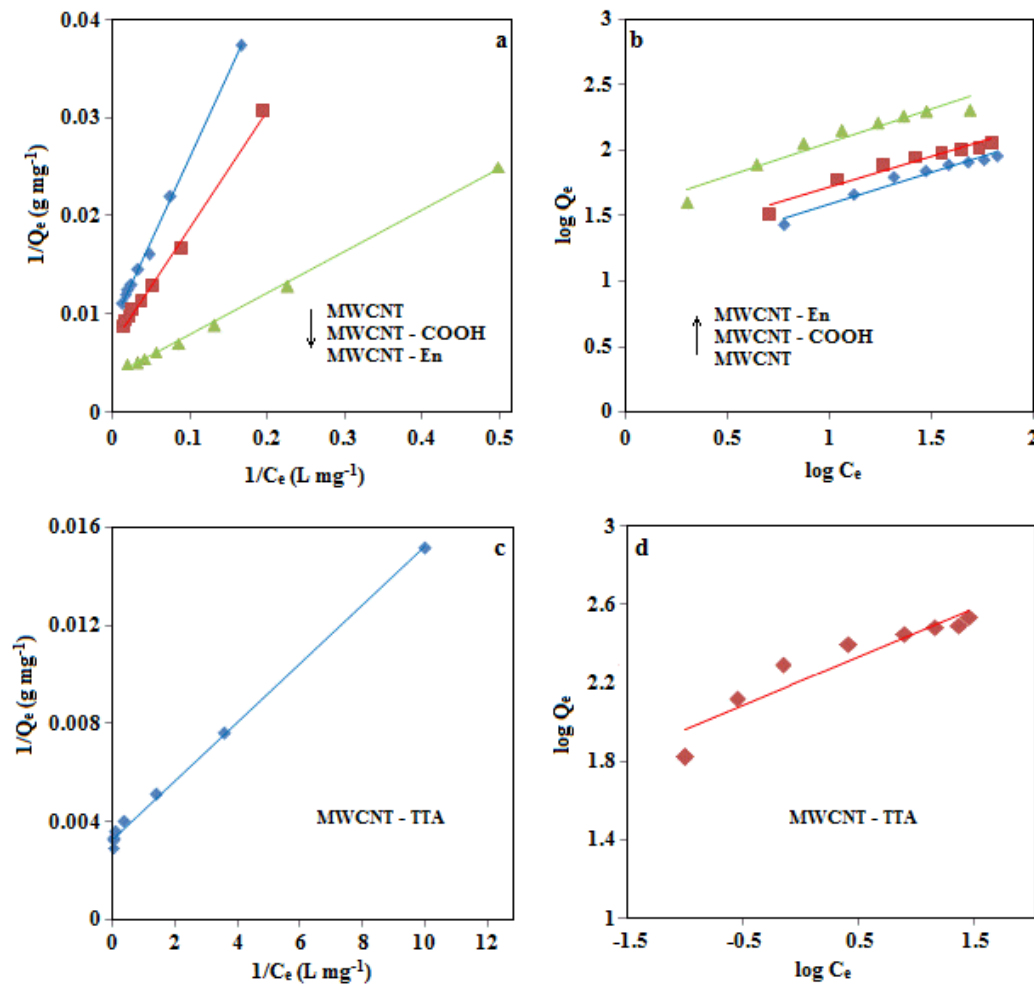


Fig. 7. The plots of Langmuir (a and c) and Freundlich (b and d) isotherm models for chromium adsorption.

Based on the results presented in Table 2 and Fig. 8, the Langmuir model has lower χ^2 values and reveals that the Langmuir model can better describe adsorption behavior of chromium(VI) on the sorbents.

3.6. Thermodynamic study

Effect of temperature on chromium(VI) adsorption was studied at initial Cr(VI) concentration of 40 mg L^{-1} , adsorbent dosage of 0.15 g L^{-1} , sample volume of 50 mL , $\text{pH} = 2.5$ and

Table 2
The data of isotherm models for chromium(VI) adsorption using as-synthesized adsorbents

Adsorbent	Langmuir				Freundlich			
	$Q_m (\text{mg g}^{-1})$	R^2	b	χ^2	n	K_f	R^2	χ^2
CNT	125.00	0.99	0.046	0.22	2.05	12.44	0.96	2.42
CNT-COOH	166.66	0.99	0.05	0.48	2.13	17.66	0.95	3.76
CNT-En	333.33	0.99	0.07	1.34	1.96	34.91	0.93	17.82
CNT-TTA	333.33	0.99	3.0	6.67	4.08	162.50	0.88	34.40

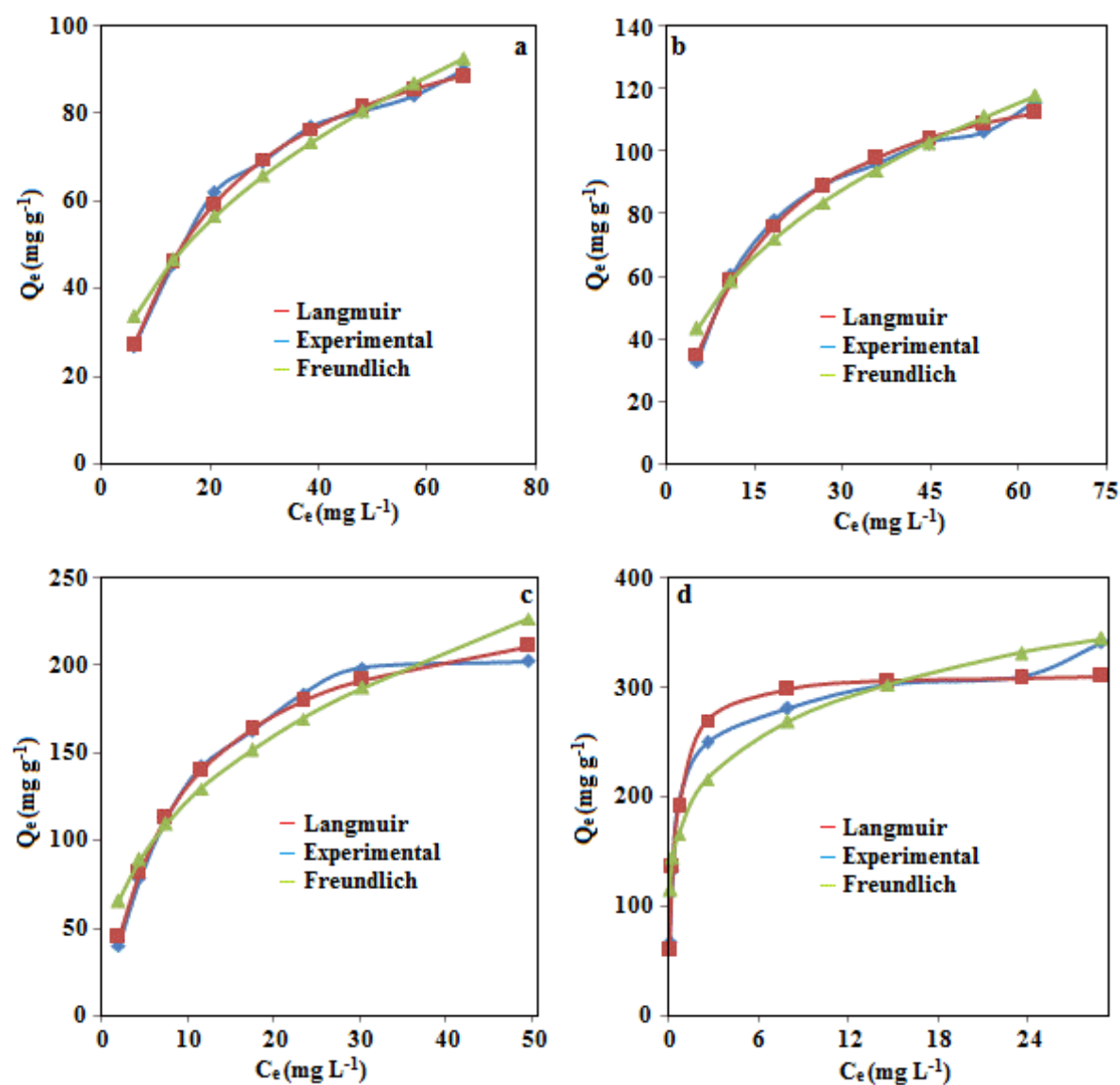


Fig. 8. Fitting experimental adsorption model with calculated value using (a) CNT, (b) oxidized CNT, (c) CNT-En, and (d) CNT-TTA.

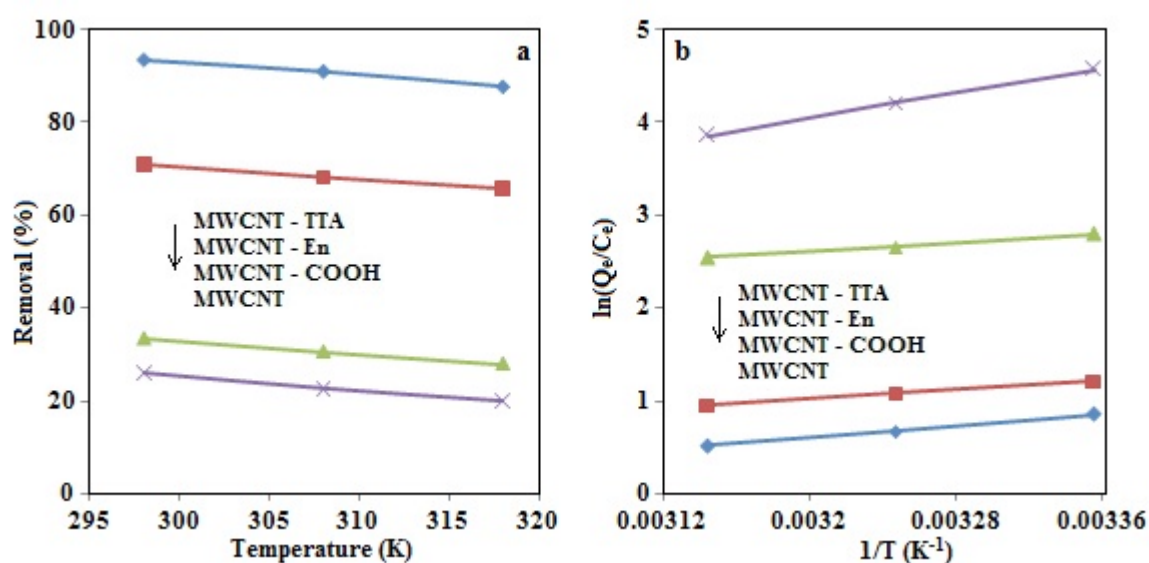


Fig. 9. Effect of temperature on (a) chromium adsorption and (b) plots of $\ln(Q_e/C_e)$ against $1/T$.

three temperatures equal to 298, 308 and 318 K. According to the results presented in Fig. 9(a), the removal percentage is decreased by increasing the temperature and indicates that the chromium(VI) adsorption onto all employed sorbents obeys an exothermic path. The thermodynamic parameters in the adsorption process, ΔH^0 (kJ mol⁻¹), ΔS^0 (JK⁻¹ mol⁻¹) and ΔG^0 (kJ mol⁻¹) could be evaluated using the equations (10)–(12), where R and T are gas constant (8.314×10^{-3} kJK⁻¹ mol⁻¹) and absolute temperature (K), respectively.

$$\Delta G^0 = -RT \ln (Q_e/C_e) \quad (10)$$

$$\Delta G^0 = \Delta H^0 - T\Delta S^0 \quad (11)$$

$$\ln (Q_e/C_e) = \Delta S^0/R - \Delta H^0/RT \quad (12)$$

The plots of $\ln (Q_e/C_e)$ versus $1/T$ are linear (Fig. 9(b)) with the slope and the intercept giving values of ΔH^0 and ΔS^0 [47–49]. The results in Table 3 exhibit that chromium(VI) adsorptions are accompanied by increase in Gibbs energies; however, the values are negative which make the interactions spontaneous and suggest that the processes are not feasible at higher temperatures. Additionally, the enthalpy changes, ΔH^0 , show negative values and confirm exothermic adsorption processes. Entropy values are also decreased for chromium(VI) adsorptions as the ΔS^0 values for the interactions are negative which indicate chromium(VI) in the solution is in more chaotic state relative to the adsorbed state.

3.7. Desorption and reusability

Regeneration or desorption of the target analyte from the sorbent material makes the sorption process more economical. Consequently, release of adsorbed chromium(VI) from sorbent surface was studied using NaOH solution as the eluent. According to results for effect of pH, the adsorption was not efficient in the alkali medium; therefore, elution with basic solution may be favorable. It was observed

Table 3

The thermodynamic data for chromium(VI) adsorption using as-synthesized adsorbents

Adsorbent	ΔG^0 (kJ mol ⁻¹)			ΔH^0 (kJ mol ⁻¹)	ΔS^0 (J k ⁻¹ mol ⁻¹)
	298 K	308 K	318 K		
CNT	-2.09	-1.71	-1.35	-13.12	-37.06
CNT-COOH	-2.99	-2.75	-2.50	-10.33	-24.6
CNT-En	-6.92	-6.80	-6.71	-10.01	-10.37
CNT-TTA	-11.3	-10.78	-10.19	-27.87	-55.46

that using 2.0 mol L⁻¹ of NaOH the release of chromium(VI) ions was quantitative (97%).

In order to evaluate the reusability of the sorbents, they were subjected to several loadings with the chromium(VI) solution and subsequent elution. It was found that after six cycles of sorption and desorption (Fig. 10), the removal efficiencies were 88.5%, 70%, 37.5% and 30% for CNT-TTA, CNT-En, CNT-COOH and raw CNT, respectively. Decrease in removal efficiencies are 6%, 8%, 16% and 23% which confirm high efficiency and appropriate stability of amine functionalized sorbents as regenerable adsorbents.

3.8. Adsorption mechanism

Chromium(VI) adsorption onto adsorbents may take place through physical, chemical or physiochemical adsorption processes. According to the kinetic and isotherm studies, chromium(VI) adsorption follows second order and Langmuir adsorption models as well as heat of adsorption is in the range of 13–28 kJ mol⁻¹. It is known that second-order model is equal to chemisorption as well as Langmuir model shows a monolayer chemisorption process; moreover, the heat of sorption in the range of 2.1–20.9 kJ mol⁻¹ confirms a physical adsorption while the heat of chemisorption is in

a range of 80–200 kJ mol⁻¹ [50]. Based on above description and according to the experimental results, chromium(VI) sorption is not a net physical or chemical interaction and is along with a physicochemical sorption process. Therefore, the mechanism of chromium(VI) adsorption is complex and both the chemical and physical adsorptions exist at the same time in the adsorption process.

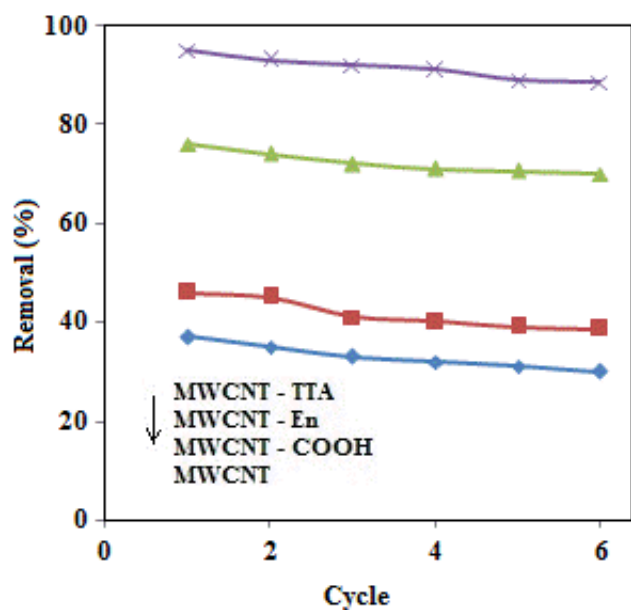


Fig. 10. The effects of reusability cycles of the adsorbents on the chromium removal efficiencies.

In this work, CNTs and amine functionalized CNTs have been employed for chromium(VI) adsorption. With precious inspection in the adsorbents structures, it can be found that oxy-hydroxy and amine groups are main functional groups in their structures. Besides, it is well known that chromium as anionic species can be adsorbed via electrostatic attraction, ligand exchange, inner and/or outer-sphere complexation and ion-exchange mechanisms. At the same time, there are electrostatic attractions between negatively charged chromium species (HCr_2O_7^- and CrO_4^{2-}) and electropositive adsorbent surface because the sorbents contain hydroxyl and amine groups, which can be protonated at the working pH. It seems that complexation reaction is also participated in the adsorption process. The adsorptive properties of oxides are due to the existence of OH and NH functional groups as chromium may be removed by complexation on the sorbent surface forming an inner/outer-sphere complex. In brief, the adsorption of chromium species could be speculated to occur through electrostatic attraction at the positively charged active sites and complexation reaction with amine groups.

3.9. Comparison with literature

A comparative study for chromium adsorption using amine functionalized sorbents examined in the present study and other sorbents is presented in Table 4. It is obvious that the performances of the prepared sorbents are in appropriate level with respect to adsorption time as well as they demonstrate satisfactory sorption capacity which is compatible with the values found in the literature; as a result, functionalized CNTs appear to be promising sorbents for the adsorption of chromium from aquatic systems. It can be seen from the results in Tables 2 and 4 that adsorption

Table 4

Comparison of chromium(VI) adsorption by the amine functionalized-MWCNTs sorbents and some adsorbents reported in literature

Adsorbent	Time (min)	Adsorption capacity (mg g ⁻¹)	Reference
Ionic liquid modified copolymer	10	74.5	[1]
Activated carbon-APBH 50	70	59	[4]
Polyaniline-cellulose	60	18.1	[5]
Iron-zirconium oxide	60	59.9	[6]
CoFe oxide	30	5.27	[7]
Magnetic polyethylenimine- poly(vinyl alcohol)	8	88.4	[8]
Polypyrrole-graphene oxide-Fe ₃ O ₄	12 h	293	[9]
MWCNTs	60	2.35	[21]
MWCNTs	120	24	[37]
Ionic liquid - MWCNTs	40	85.83	[38]
Oxidized MWCNTs	280 h	4.2	[44]
Activated carbon - MWCNTs	60	9	[45]
MWCNTs - Fe ₃ O ₄	13 h	12.53	[49]
Egg-shell MWCNTs	30	125	This study
Oxidized MWCNTs	30	166.66	This study
Amine functionalized-MWCNTs	30	333.3	This study

capacity of raw CNT, prepared in this work, is the highest among those of the same adsorbents. This may be owing to the presence of egg-shell (CaCO_3) in CNT structure which increases the efficiency of CNT for chromium adsorption. Moreover, it is obvious that oxidized CNT shows high adsorption efficiency, too originating from high disorders in CNT structure (confirmed by Raman and TEM analysis) which offers an appropriate situation for increasing acidic functional groups on the CNT surface by acid treatment. It is observable that amine functionalized sorbent has the highest efficiency among all of the reported adsorbents which confirms functionalized CNT is a promising sorbent for the adsorption of chromium from aquatic systems.

4. Conclusions

This study demonstrated synthesis of MWCNTs (using egg-shell supported iron(0) as an efficient catalyst) and amine functionalized MWCNTs for application in the chromium(VI) adsorption process. Results obtained from chromium(VI) ion adsorption experiments showed that efficient magnetic adsorbents were successfully generated by the method. The amine functionalization improved the adsorption properties of CNTs, making the surface more suitable for chromium(VI) ion adsorption because adsorption capacity for chromium ions was two times higher than that of the oxidized CNTs. The kinetics adsorption on the oxidized and functionalized adsorbents revealed that the amine functionalized sorbents followed the second-order kinetics; however, raw CNTs obeyed the first-order model. Moreover, the adsorption process followed Langmuir isotherm model. Consequently, amine functionalized CNTs are suggested as promising materials with potential application as adsorbents in the water treatment process.

Acknowledgments

The financial support of this work by the Research Council of Amirkabir University of Technology (Tehran Polytechnic), Tehran, Iran, is gratefully acknowledged.

References

- [1] Y. Jiang, F. Li, G. Ding, Y. Chen, Y. Liu, Y. Hong, P. Liu, X. Qi, L. Ni, Synthesis of a novel ionic liquid modified copolymer hydrogel and its rapid removal of Cr(VI) from aqueous solution, *J. Colloid Interf. Sci.*, 455 (2015) 125–133.
- [2] Z. Wen, Y. Zhang, C. Dai, Z. Sun, Nanocasted synthesis of magnetic mesoporous iron cerium bimetal oxides (MMIC) as an efficient heterogeneous Fenton-like catalyst for oxidation of arsenite, *J. Hazard. Mater.*, 287 (2015) 225–233.
- [3] A. Maleki, B. Hayati, M. Naghizadeh, S.W. Joo, Adsorption of hexavalent chromium by metal organic frameworks from aqueous solution, *J. Ind. Eng. Chem.*, 28 (2015) 211–216.
- [4] M. Bhaumik, S. Agarwal, V.K. Gupta, A. Maity, Enhanced removal of Cr(VI) from aqueous solutions using polypyrrole wrapped oxidized MWCNTs nanocomposites adsorbent, *J. Colloid Interf. Sci.*, 470 (2016) 257–267.
- [5] B. Qiu, C. Xu, D. Sun, Q. Wang, H. Gao, X. Zhang, B.L. Weeks, J. Hoppera, T.C. Hoa, Z. Guoa, S. Wei, Polyaniline coating with various substrates for hexavalent chromium removal, *Appl. Surf. Sci.*, 334 (2015) 7–14.
- [6] Y. Wang, D. Liu, J. Lu, J. Huang, Enhanced adsorption of hexavalent chromium from aqueous solutions on facilely synthesized mesoporous iron–zirconium bimetal oxide, *Colloid. Surf. A: Physicochem. Eng. Asp.*, 481 (2015) 133–142.
- [7] X. Ge, C.D. Gu, X.L. Wang, J.P. Tu, Spinel type CoFe oxide porous nanosheets as magnetic adsorbents with fast removal ability and facile separation, *J. Colloid Interf. Sci.*, 454 (2015) 134–143.
- [8] X. Sun, L. Yang, Q. Li, Z. Liu, T. Dong, H. Liu, Polyethylenimine-functionalized poly(vinyl alcohol) magnetic microspheres as a novel adsorbent for rapid removal of Cr(VI) from aqueous solution, *Chem. Eng. J.*, 262 (2015) 101–108.
- [9] H. Wang, X. Yuan, Y. Wu, X. Chen, L. Leng, H. Wang, H. Li, G. Zeng, Facile synthesis of polypyrrole decorated reduced graphene oxide– Fe_3O_4 magnetic composites and its application for the Cr(VI) removal, *Chem. Eng. J.*, 262 (2015) 597–606.
- [10] A. Kaur, U. Gupta, A review on applications of nanoparticles for the preconcentration of environmental pollutants, *J. Mater. Chem.*, 19 (2009) 8279–8289.
- [11] A. Jaiswal, R. Mani, S. Banerjee, R.K. Gautam, M.C. Chattopadhyaya, Synthesis of novel nano-layered double hydroxide by urea hydrolysis method and their application in removal of chromium(VI) from aqueous solution: kinetic, thermodynamic and equilibrium studies, *J. Mol. Liquids*, 202 (2015) 52–61.
- [12] C.T. Gore, S. Omwoma, W. Chen, Y.-F. Song, Interweaved LDH/PAN nanocomposite films: application in the design of effective hexavalent chromium adsorption technology, *Chem. Eng. J.*, 284 (2016) 794–801.
- [13] T. Sathvika, Manasi, V. Rajesh, N. Rajesh, Microwave assisted immobilization of yeast in cellulose biopolymer as a green adsorbent for the sequestration of chromium, *Chem. Eng. J.*, 279 (2015) 38–46.
- [14] A.E. Chávez-Guajardo, J.C. Medina-Llamas, L. Maqueira, C.A.S. Andrade, K.G.B. Alves, C.P. de Melo, Efficient removal of Cr(VI) and Cu(II) ions from aqueous media by use of polypyrrole/maghemite and polyaniline/maghemite magnetic nanocomposites, *Chem. Eng. J.*, 281 (2015) 826–836.
- [15] P. Khare, A. Yadav, J. Ramkumar, N. Verma, Microchannel-embedded metal–carbon–polymer nanocomposite as a novel support for chitosan for efficient removal of hexavalent chromium from water under dynamic conditions, *Chem. Eng. J.*, 293 (2016) 44–54.
- [16] K. Singh, J.K. Arora, T.J.M. Sinha, S. Srivastava, Functionalization of nanocrystalline cellulose for decontamination of Cr(III) and Cr(VI) from aqueous system: computational modeling approach, *Clean Technol. Environ. Policy*, 16 (2014) 1179–1191.
- [17] S. Kalidhasan, A.S.K. Kumar, V. Rajesh, N. Rajesh, Enhanced adsorption of hexavalent chromium arising out of an admirable interaction between a synthetic polymer and an ionic liquid, *Chem. Eng. J.*, 222 (2013) 454–463.
- [18] Z. Jiang, Y. Liu, G. Zeng, W. Xu, B. Zheng, X. Tan, S. Wang, Adsorption of hexavalent chromium by polyacrylonitrile (PAN)-based activated carbon fibers from aqueous solution, *RSC Adv.*, 5 (2015) 25389–25397.
- [19] C. Luo, Z. Tian, B. Yang, L. Zhang, S. Yan, Manganese dioxide/iron oxide/acid oxidized multi-walled carbon nanotube magnetic nanocomposite for enhanced hexavalent chromium removal, *Chem. Eng. J.*, 234 (2013) 256–265.
- [20] M.K. Kim, K.S. Sundaram, G.A. Iyengar, K.-P. Lee, A novel chitosan functional gel included with multiwall carbon nanotube and substituted polyaniline as adsorbent for efficient removal of chromium ion, *Chem. Eng. J.*, 267 (2015) 51–64.
- [21] Y.-L. Yu, Y.-T. Zhuang, X.-Y. Song, J.-H. Wang, Lyophilized carbon nanotubes/graphene oxide modified cigarette filter for the effective removal of cadmium and chromium from mainstream smoke, *Chem. Eng. J.*, 280 (2015) 58–65.
- [22] J. Hu, C. Chen, X. Zhu, X. Wang, Removal of chromium from aqueous solution by using oxidized multiwalled carbon nanotubes, *J. Hazard. Mater.*, 162 (2009) 1542–1550.
- [23] A.A. Ihsanullah, A.M. Al-Amer, T. Laoui, M.J. Al-Marri, M.S. Nasser, M. Khraisheh, M.A. Atieh, Heavy metal removal

- from aqueous solution by advanced carbon nanotubes: critical review of adsorption applications, *Sep. Pur. Technol.*, 157 (2016) 141–161.
- [24] M. Singh, S. Vinodh Kumar, S.A. Waghmare, P.D. Sabale, Aragonite–vaterite–calcite: polymorphs of CaCO_3 in 7th century CE lime plasters of Alampur group of temples, India, *Construct. Build. Mater.*, 112 (2016) 386–397.
- [25] S. Mishra, S.H. Sonawane, R.P. Singh, Studies on characterization of nano CaCO_3 Prepared by the in situ deposition technique and its application in PP-nano CaCO_3 composites, *J. Polym. Sci. Part B: Polym. Phys.*, 43 (2005) 107–113.
- [26] S. Yuan, Z. Zhou, G. Li, Structural evolution from mesoporous $\alpha\text{-Fe}_2\text{O}_3$ to $\text{Fe}_3\text{O}_4@\text{C}$ and $\gamma\text{-Fe}_2\text{O}_3$ nanospheres and their lithium storage performances, *Cryst. Eng. Comm.*, 13 (2011) 4709–4713.
- [27] Q.-G. Zhu, A.N.A. Sujari, S.A. Ghani, MWCNT modified composite pencil graphite electrodes fabricated by direct dripping and electrophoretic deposition methods: a comparison study, *J. Electrochem. Soc.*, 160 (2013) B23–B29.
- [28] J. Kim, M.K. Chung, B.H. Ka, J.H. Ku, S. Park, J. Ryu, S.M. Oh, The role of metallic Fe and carbon matrix in $\text{Fe}_2\text{O}_3/\text{Fe}$ /carbon nanocomposite for lithium-ion batteries, *J. Electrochem. Soc.*, 157 (2010) A412–A417.
- [29] E.-S.M. Duraia, M. Burkitbaev, H. Mohamedbakr, Z. Mansurov, S. Tokmolden, G.W. Beall, Growth of carbon nanotubes on diatomite, *Vacuum*, 84 (2010) 464–468.
- [30] W. Li, H. Zhang, C. Wang, Y. Zhang, L. Xu, K. Zhu, S. Xie, Raman characterization of aligned carbon nanotubes produced by thermal decomposition of hydrocarbon vapor, *Appl. Phys. Lett.*, 70 (1997) 2684.
- [31] S.J. Sung, T. Kim, S.J. Yang, J.Y. Oh, C.R. Park, New insights into the oxidation of single-walled carbon nanotubes for the fabrication of transparent conductive films, *Carbon*, 81 (2015) 525–534.
- [32] B. Bahrami, A. Khodadadi, Y. Mortazavib, M. Esmaili, Short time synthesis of high quality carbon nanotubes with high rates by CVD of methane on continuously emerged iron nanoparticles, *Appl. Surf. Sci.*, 257 (2011) 9710–9716.
- [33] Y. Wang, L. Shi, L. Gao, Q. Wei, L. Cui, L. Hu, L. Yan, B. Du, The removal of lead ions from aqueous solution by using magnetic hydroxypropyl chitosan/oxidized multiwalled carbon nanotubes composites, *J. Colloid Interf. Sci.*, 451 (2015) 7–14.
- [34] H. Alijani, M.H. Beyki, S.N. Mirzababaei, Adsorption of UO_2^{2+} ions from aqueous solution using amine functionalized MWCNT: kinetic, thermodynamic and isotherm study, *J. Radioanal. Nucl. Chem.*, 306 (2015) 165–173.
- [35] G. Wang, J. Chen, Y. Tian, Y. Jin, Y. Li, Water assisted synthesis of double-walled carbon nanotubes with a narrow diameter distribution from methane over a Co–Mo/MgO catalyst, *Catal. Today*, 183 (2012) 26–33.
- [36] X.-H. Wang, F.-F. Liu, L. Lu, S. Yang, Y. Zhao, L.-B. Sun, S.-G. Wang, Individual and competitive adsorption of Cr(VI) and phosphate onto synthetic Fe–Al hydroxides, *Colloid. Surf. A Physicochem. Eng. Asp.*, 423 (2013) 42–49.
- [37] A. Ahmadpour, N. Eftekhari, A. Ayati, Performance of MWCNTs and a low-cost adsorbent for Chromium(VI) ion removal, *J. Nanostruct. Chem.*, 4 (2014) 171–178.
- [38] A.S. Krishna Kumar, S.-J. Jiang, W.-L. Tseng, Effective adsorption of chromium(VI)/Cr(III) from aqueous solution using ionic liquid functionalized multiwalled carbon nanotube as a super sorbent, *J. Mater. Chem. A*, 3 (2015) 7044–7057.
- [39] C. Jung, J. Heo, J. Han, N. Her, S.-J. Lee, J. Oh, J. Ryu, Y. Yoon, Hexavalent chromium removal by various adsorbents: powdered activated carbon, chitosan, and single/multi-walled carbon nanotubes, *Sep. Pur. Technol.*, 106 (2013) 63–71.
- [40] Y. Li, L. Cao, L. Li, C. Yang, In situ growing directional spindle TiO_2 nanocrystals on cellulose fibers for enhanced Pb^{2+} adsorption from water, *J. Hazard. Mater.*, 289 (2015) 140–148.
- [41] S. Pan, J. Li, G. Wana, C. Liu, W. Fan, L. Wang, Nanosized yolk-shell $\text{Fe}_3\text{O}_4@\text{Zr}(\text{OH})_x$ spheres for efficient removal of Pb(II) from aqueous solution, *J. Hazard. Mater.*, 309 (2016) 1–9.
- [42] S. Rahimi, R.M. Moattari, L. Rajabi, A.A. Derakhshan, M. Keyhani, Iron oxide/hydroxide ($\alpha,\gamma\text{-FeOOH}$) nanoparticles as high potential adsorbents for lead removal from polluted aquatic media, *J. Ind. Eng. Chem.*, 23 (2015) 33–43.
- [43] K. Kalantari, M.B. Ahmad, H.R.F. Masoumi, K. Shamel, M. Basri, R. Khandanlou, Rapid and high capacity adsorption of heavy metals by $\text{Fe}_3\text{O}_4/\text{montmorillonite}$ nanocomposite using response surface methodology: preparation, characterization, optimization, equilibrium isotherms, and adsorption kinetics study, *J. Taiwan Inst. Chem. Eng.*, 49 (2015) 192–198.
- [44] J. Hu, C. Chen, X. Zhu, X. Wang, Removal of chromium from aqueous solution by using oxidized multiwalled carbon nanotubes, *J. Hazard. Mater.*, 162 (2009) 1542–1550.
- [45] M. Ali Atieh, Removal of Chromium (VI) from polluted water using carbon nanotubes supported with activated carbon, *Procedia Environ. Sci.*, 4 (2011) 281–293.
- [46] M.H. Beyki, F. Shemirani, Dual application of facilely synthesized Fe_3O_4 nanoparticles: fast reduction of nitro compound and preparation of magnetic polyphenylthiourea nanocomposite for efficient adsorption of lead ions, *RSC Adv.*, 5 (2015) 22224–22233.
- [47] M.H. Baki, F. Shemirani, R. Khani, M. Bayat, Applicability of diclofenac–montmorillonite as a selective sorbent for adsorption of palladium(II); kinetic and thermodynamic studies, *Anal. Method.*, 6 (2014) 1875–1883.
- [48] R. Khani, S. Sobhani, M.H. Beyki, Highly selective and efficient removal of lead with magnetic nano-adsorbent: multivariate optimization, isotherm and thermodynamic studies, *J. Colloid Interf. Sci.*, 466 (2016) 198–205.
- [49] Z.-N. Huang, X.-L. Wang, D.-S. Yang, Adsorption of Cr(VI) in wastewater using magnetic multi-wall carbon nanotubes, *Water Sci. Eng.*, 8 (2015) 226–232.
- [50] H. Alijani, Z. Shariatinia, A. Aroujalian Mashhadi, Water assisted synthesis of MWCNTs over natural magnetic rock: an effective magnetic adsorbent with enhanced mercury(II) adsorption property, *Chem. Eng. J.*, 281 (2015) 468–481.